Turbulence modulation by variable density and viscosity

By A. Patel†, R. Pecnik†, J. W. R. Peeters†, S. Hickel† AND M. E. Moghadam

We investigate the effectiveness of the semi-local Reynolds number $\mathrm{Re}_\tau^\star$ to parametrize wall-bounded flows with strong density, ρ, and viscosity, μ, gradients. Several cases are considered, namely, volumetrically heated low-Mach-number turbulent channel flows, a simultaneously heated and cooled flow with CO_2 at supercritical pressure, and heated and cooled supersonic boundary layer flows. The mean density and viscosity in some of these cases vary up to a factor of nine and six, respectively. We show that, even for such high gradients in mean properties, the velocity transformation based on the semi-local Reynolds number is able to collapse the mean streamwise velocity profiles. We furthermore provide evidence that the turbulent kinetic energy and streamwise vorticity budget equations are also governed by the semi-local Reynolds number. For cases with strong property variations, additional mechanisms appear that are caused by individual density (e.g., baroclinicity) or viscosity gradients. However, in the cases investigated herein, these additional mechanisms are small. The insights gained are used to improve a wall model, which is then tested in a wall-modeled large-eddy simulation (LES) of a compressible channel flow with isothermal walls.

1. Introduction

Turbulent flows with variable thermophysical properties are common in supersonic flows, in low-Mach-number flows with strong wall heating or cooling, and in reacting flows. In such cases the effects of thermophysical property variations can be strong enough to modulate turbulence (Coleman *et al.* 1995; Foysi *et al.* 2004; Duan *et al.* 2010; Lee *et al.* 2013; Modesti & Pirozzoli 2016). Furthermore, in the past decade, there has been an increased interest in heated and cooled fluids at supercritical pressure for novel thermodynamic power cycles or rocket propulsion systems. Fluids slightly above the supercritical pressure and close to the pseudo-critical temperature pose strong thermophysical property variations due to a combination of strong dependence of properties with temperature and large molecular Prandtl numbers (Peeters *et al.* 2016; Nemati *et al.* 2016). The strong thermophysical property variations can alter the conventional behavior of turbulence and make conventional scaling laws for constant-property flows fail. Moreover, the physical mechanisms that lead to turbulence modulation are not yet well understood.

For incompressible constant-property flows, the most important parameter in the description of turbulent boundary layers is the Reynolds number. For compressible flows, the Mach number and the associated changes in properties become additional parameters that characterize turbulent wall-bounded flows. From past studies, it is known that differences between a supersonic flow and a constant-property flow can be explained by simply accounting for the mean fluid property variations, as long as the Mach number,

† Delft University of Technology, The Netherlands

M, associated with the turbulent fluctuations remains small ($\mathrm{M}' < 0.3$; Smits & Dussauge 2006). This result is known as Morkovin's hypothesis (Morkovin 1962).

In our recent work (Patel *et al.* 2015) we provide a mathematical basis for the use of the semi-local scaling as proposed by Huang *et al.* (1995) based on heuristic arguments. The main conclusion is that under the limit of small property fluctuations in highly turbulent flows, a change in turbulent structure is strongly governed by the wall-normal gradient of the semi-local Reynolds number, $\mathrm{Re}_\tau^\star \equiv \sqrt{(\overline{\rho}/\overline{\rho}_w)}/(\overline{\mu}/\overline{\mu}_w)\ \mathrm{Re}_\tau$, and not by individual mean density or viscosity gradients (the bar denotes Reynolds averaging, subscript w indicates the value at the wall, and Re_τ is the friction Reynolds number based on wall quantities and the half channel height, h). Thus, $\mathrm{Re}_\tau^\star$ provides a scaling parameter that accounts for the influence of variable properties on turbulent boundary layers.

The van Driest velocity transformation $\overline{u}^{\mathrm{vD}} = \int_0^{\overline{u}^+} \sqrt{(\overline{\rho}/\overline{\rho}_w)}d\overline{u}^+$ (superscript + denotes the classical wall-based scaling $\overline{u}^+ = \overline{u}/u_\tau$, with u_τ the friction velocity), which has been successfully applied for adiabatic compressible boundary layers to collapse velocity profiles onto incompressible results, accounts for the changes in velocity scales by using a density-weighted transformation, but it assumes that the viscous length scale is similar to an incompressible boundary layer (Smits & Dussauge 2006). We recently derived an extension of the van Driest transformation using the semi-local Reynolds number $\mathrm{Re}_\tau^\star$ to account for changes in viscous length scales (Patel *et al.* 2016). A mathematically equivalent transformation was earlier derived by Trettel & Larsson (2016) using different arguments, where they also highlight the importance of accounting for changes in viscous length scales.

The first objective of the present work is to test the validity of the extended van Driest transformation on a range of turbulent flows with strong density/viscosity gradients, such as volumetrically heated channel flows, heated or cooled flows with fluids at supercritical pressure and supersonic boundary layer flows. We also investigate the effectiveness of $\mathrm{Re}_\tau^\star$ as a scaling parameter for cases with very large gradients in density/viscosity, and we discuss the significance of additional physical mechanisms that occur due to these strong gradients. Finally, we will use the semi-local scaling methods to correct a simple mixing length eddy viscosity model that can be used in wall-modeled large-eddy simulations (LES) of compressible flows.

2. Methodology and turbulent flow cases

The channel flow cases have been obtained using our own in-house DNS solver of the low-Mach-number approximation of the Navier-Stokes equations. Gradients in temperature are obtained by heating the flow using a constant volumetric heat source in the energy equation and by applying isothermal boundary conditions at both walls. Different constitutive relations for density, ρ, and viscosity, μ, as a function of temperature, T, are used. The details of all investigated cases are outlined in Table 1. The constitutive relations for density and viscosity as a function of temperature are listed in the second and third columns, respectively. The following columns report the wall-based friction Reynolds number, Re_τ; the semi-local Reynolds number at the channel center, $\mathrm{Re}_{\tau c}^\star = \sqrt{(\overline{\rho}_c/\overline{\rho}_w)}/(\overline{\mu}_c/\overline{\mu}_w)\ \mathrm{Re}_\tau$ (subscript c denotes the value at channel center); and the number of mesh points, N, and the length of the domain, L, in streamwise, x, wall-normal, y, and spanwise, z, directions. The last column shows the wall heat flux parameter, $B_q = q_w/(\overline{\rho}_w c_p u_\tau T_w)$ (where q_w is the wall heat flux and c_p is the specific heat at constant pressure).

Case	ρ/ρ_w	μ/μ_w	Re_τ	$\mathrm{Re}^*_{\tau_c}$	$N_x \times N_y \times N_z$	$L_x \times L_y \times L_z$	B_q
CP395	1	1	395	395	$240 \times 264 \times 240$	$2\pi h \times 2h \times \pi h$	0
$\mathrm{CRe}^*_\tau 1$	$(T/T_w)^{-1}$	$(T/T_w)^{-0.5}$	395	395	$240 \times 264 \times 240$	$2\pi h \times 2h \times \pi h$	-0.044
$\mathrm{CRe}^*_\tau 2$	$(T/T_w)^{-1}$	$(T/T_w)^{-0.5}$	395	395	$288 \times 264 \times 288$	$2\pi h \times 2h \times \pi h$	-0.137
$\mathrm{CRe}^*_\tau 3$	$(T/T_w)^{-1}$	$(T/T_w)^{-0.5}$	395	395	$288 \times 312 \times 288$	$2\pi h \times 2h \times \pi h$	-0.24
GL	$(T/T_w)^{-1}$	$(T/T_w)^{0.7}$	950	137	$360 \times 360 \times 360$	$4\pi h \times 2h \times 1.5\pi h$	-0.079
LL	1	$(T/T_w)^{-1}$	150	943	$360 \times 312 \times 360$	$2\pi h \times 2h \times \pi h$	-0.413

TABLE 1. Parameters for the simulated cases. CP395 – constant-property case with $\mathrm{Re}_\tau = 395$; $\mathrm{CRe}^*_\tau 1$, $\mathrm{CRe}^*_\tau 2$, $\mathrm{CRe}^*_\tau 3$ – variable-property cases with constant Re^*_τ (= 395) across the channel height; GL – case with gas-like property variations; LL – case with liquid-like property variations.

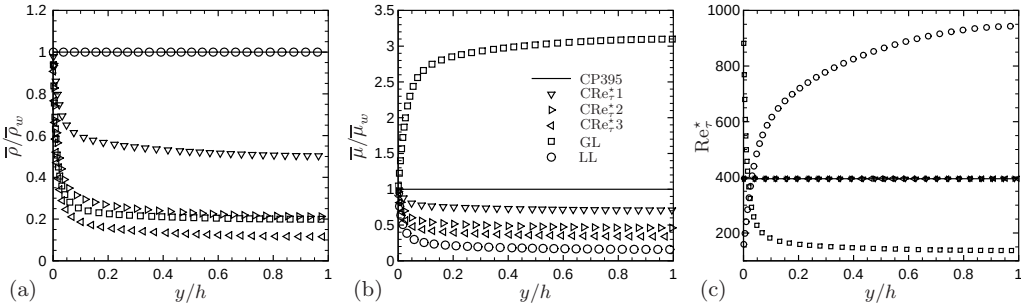

FIGURE 1. (a) Density $\overline{\rho}/\overline{\rho}_w$, (b) viscosity $\overline{\mu}/\overline{\mu}_w$, and (c) semi-local Reynolds number $\mathrm{Re}^\star_\tau$.

The case CP395 corresponds to a constant-property case with $\mathrm{Re}_\tau = 395$. Cases $\mathrm{CRe}^\star_\tau 1$, $\mathrm{CRe}^\star_\tau 2$ and $\mathrm{CRe}^\star_\tau 3$ are flows with increasing mean gradients (increasing B_q) in density and viscosity, but such that the semi-local Reynolds number $\mathrm{Re}^\star_\tau$ is constant across the whole channel height (meaning $\sqrt{\overline{\rho}/\overline{\rho}_w} = \overline{\mu}/\overline{\mu}_w$). These cases have been simulated to test the efficacy of $\mathrm{Re}^\star_\tau$ as a scaling parameter. The density gradients increase from $\overline{\rho}_w/\overline{\rho}_c \approx 2$ for case $\mathrm{CRe}^\star_\tau 1$ to $\overline{\rho}_w/\overline{\rho}_c \approx 9$ for case $\mathrm{CRe}^\star_\tau 3$. Cases GL and LL are flows with gas-like and liquid-like property variations that have large gradients in $Re^\star_\tau$. Cases CP395 and $\mathrm{CRe}^\star_\tau 1$ were also studied in Patel *et al.* (2015, 2016) and are used here as a reference. The corresponding plots of mean density, viscosity and $\mathrm{Re}^\star_\tau$ are shown in Figure 1. The relative property fluctuations ${\rho'}_{rms}/\overline{\rho}$ and ${\mu'}_{rms}/\overline{\mu}$ (prime denotes Reynolds-averaged fluctuations, and the subscript rms indicates the root mean square value) for the cases with very large property variations reach a value of about 0.25. The details on the governing equations and the numerical schemes can be found in Patel *et al.* (2015). For cases $\mathrm{CRe}^\star_\tau 2$, $\mathrm{CRe}^\star_\tau 3$ and GL with large density gradients, we used a two-step predictor-corrector time integration scheme (Najm *et al.* 1998) to increase the numerical stability. The velocity components along the x, y and z directions are denoted as u, v and w.

The second dataset is a DNS of a turbulent flow with CO_2 at supercritical pressure ($scCO_2$) in an annulus with a hot inner wall and a cold outer wall (Peeters *et al.* 2016). The pseudo-critical temperature, at which the thermophysical properties change from a liquid-like state to a gas-like state, is close to the heated inner wall. The transition results in strong thermophysical property variations, accompanied by a five-fold increase in the molecular Prandtl number. The third database corresponds to a heated/cooled supersonic boundary layer from Shadloo *et al.* (2015).

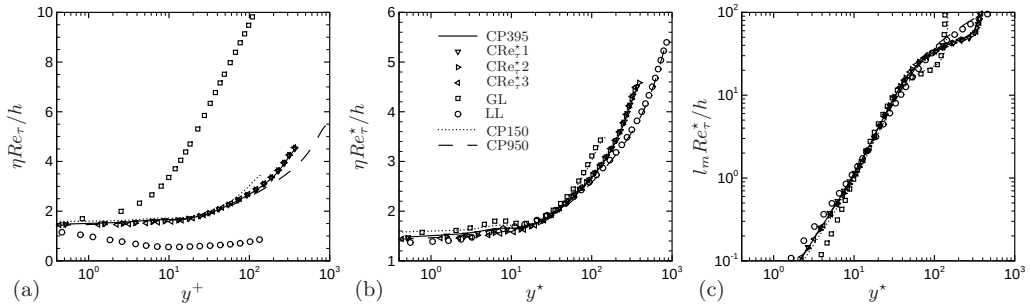

FIGURE 2. (a) Kolmogorov length scale in terms of wall-based viscous units, and (b) Kolmogorov length scale and (c) mixing length in terms of semi-local viscous units. Two additional constant-property flows with $\mathrm{Re}_\tau = 150$ (CP150) and $\mathrm{Re}_\tau = 950$ (CP950) are shown to depict Reynolds number effects in the outer layer.

3. Results

First, we highlight the change in length scales due to mean property variations and how $\mathrm{Re}^\star_\tau$ provides a good measure of it. Second, we highlight some structural changes due to gradients in $\mathrm{Re}^\star_\tau$. Third, we discuss the significance of some additional mechanisms that are not governed by $\mathrm{Re}^\star_\tau$ and that occur because of property fluctuations and very strong density/viscosity gradients. Finally, wall-modeled LES of a compressible channel flow with cold walls is performed by taking into account the change in characteristic length scales due to $\mathrm{Re}^\star_\tau$ gradients.

3.1. *Length scales and mean velocity scaling*

As pointed out in Section 1, near-wall property gradients could possibly cause a change in viscous length scales. Figure 2(a) shows the Kolmogorov length scale $\eta = ((\overline{\mu}/\overline{\rho})^3\overline{\rho}/\epsilon_k)^{0.25}$ (here ϵ_k is the turbulent kinetic energy dissipation rate per unit volume) normalized by the wall-based viscous length scale $\delta_v^+ = h/\mathrm{Re}_\tau$ and plotted as a function of $y^+ = y/\delta_v^+$. η normalized in terms of semi-local viscous units ($\delta_v^\star = h/\mathrm{Re}^\star_\tau$) and plotted as a function of semi-local wall distance $y^\star = y/\delta_v^\star$ is shown in Figure 2(b). It can be seen that cases with gradients in $\mathrm{Re}^\star_\tau$ show strong deviations in η when normalized using classical wall-based units. On the other hand, η can be collapsed when using semi-local length scales. Note, for cases with constant $\mathrm{Re}^\star_\tau$, the semi-local scaling is equivalent to the wall-based scaling. Similar observations can be made for the mixing length, which is defined as

$$l_m^2 = -\widetilde{u''v''}/(d\overline{u}/dy)^2, \tag{3.1}$$

where the tilde denotes Favre averaging and the double prime indicates the corresponding fluctuations. Figure 2(c) shows the mixing length normalized and plotted in terms of semi-local units and a good collapse is obtained in the entire inner layer, except very close to wall ($y^\star < 10$) where cases with $\mathrm{Re}^\star_\tau$ gradients show deviations. However, for $y^\star < 10$, l_m is small and the flow is dominated by viscosity. The suggested scaling of l_m in Figure 2(c) can be naturally obtained from the streamwise stress-balance equation, which, after neglecting the viscosity fluctuations, can be written as

$$-\frac{\overline{\rho}\widetilde{u''v''}}{\tau_w} + \frac{h}{\mathrm{Re}_\tau}\left(\frac{\overline{\mu}}{\overline{\mu}_w}\right)\frac{d\overline{u}^+}{dy} \approx \frac{\tau}{\tau_w} = \left(1 - \frac{y}{h}\right), \tag{3.2}$$

where τ and τ_w represent the total and wall shear stress, respectively. Substituting Eq. (3.1) into Eq. (3.2) results in a quadratic equation for $d\overline{u}^+/dy$, which, after solv-

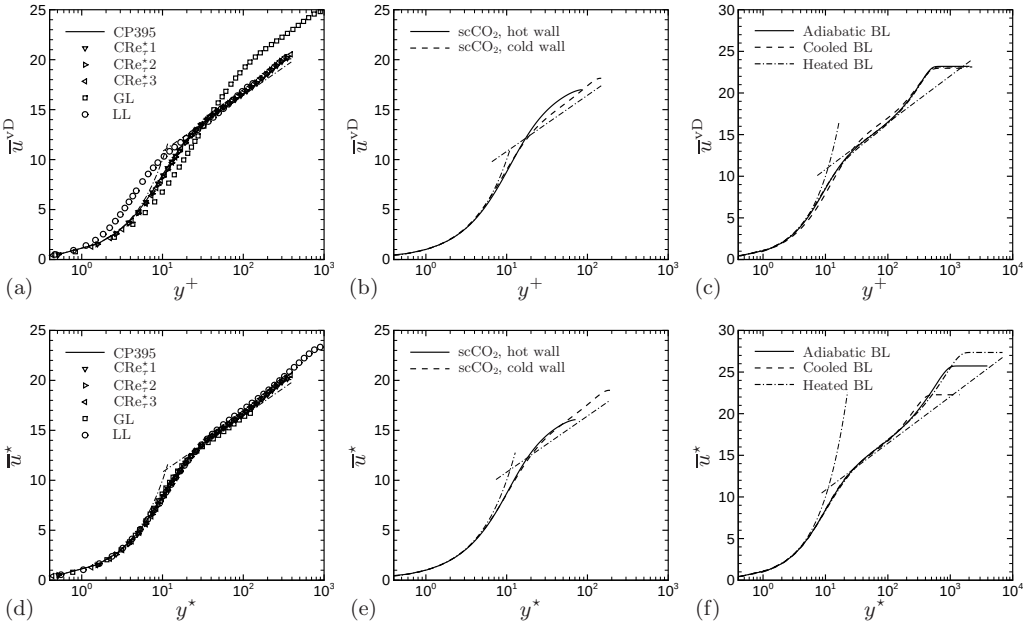

FIGURE 3. (a,b,c) van Driest–transformed velocity $\overline{u}^{\mathrm{vD}}$ as a function of y^+, (d,e,f) extended van Driest–transformed velocity $\overline{u}^\star$ as a function of $y^\star$. (a,d) Cases CP395, CRe$_\tau^\star$1, CRe$_\tau^\star$2, CRe$_\tau^\star$3, GL and LL; (b,e) scCO$_2$ cases from Peeters *et al.* (2016); (c,f) heated, cooled and adiabatic supersonic boundary layers from Shadloo *et al.* (2015). The thin dash-dotted lines indicate the linear and log-law velocity profiles.

ing and simplifying, can be written as

$$\frac{h}{\mathrm{Re}_\tau^\star}\frac{d\overline{u}^{\mathrm{vD}}}{dy} = \frac{2\tau/\tau_w}{1+\sqrt{1+4\tau/\tau_w\left(l_m \mathrm{Re}_\tau^\star/h\right)^2}}. \tag{3.3}$$

The good collapse of l_m in terms of semi-local units can also be exploited to derive the extended van Driest transformation as

$$d\overline{u}^\star = \left(1+\frac{y}{\mathrm{Re}_\tau^\star}\frac{d\mathrm{Re}_\tau^\star}{dy}\right) d\overline{u}^{\mathrm{vD}}. \tag{3.4}$$

For a more detailed description of the derivation refer to Patel *et al.* (2016). The transformation proposed by Trettel & Larsson (2016) is equivalent to Eq. (3.4) and can be obtained by substituting the definitions of $\mathrm{Re}_\tau^\star$ and $\overline{u}^{\mathrm{vD}}$.

The velocity transformation is applied to the cases described in Section 2. The van Driest–transformed velocity, $\overline{u}^{\mathrm{vD}}$, is plotted as a function of y^+ in Figure 3(a-c), and the extended velocity transformation, $\overline{u}^\star$, is plotted as a function of $y^\star$ in Figure 3(d-f). $\overline{u}^{\mathrm{vD}}$ for cases with constant $\mathrm{Re}_\tau^\star$ profiles follow the incompressible velocity profile closely. However, $\overline{u}^{\mathrm{vD}}$ deviates for cases with gradients in $\mathrm{Re}_\tau^\star$ in Figure 3(a), while all $\overline{u}^\star$ profiles show a collapse in Figure 3(d). For the flow with CO_2 at supercritical pressure in an annulus (Peeters *et al.* 2016) in Figure 3(b,e), the velocity profile is split into two profiles corresponding to the hot and cold walls. Using $\overline{u}^{\mathrm{vD}}$ shows a slight deviation among the two profiles, while a good collapse is obtained using the $u^\star$ transformation. The cooled and heated supersonic boundary layers compared to an adiabatic case (Shadloo *et al.* 2015) is shown in Figure 3(c,f). While the $\overline{u}^{\mathrm{vD}}$ for adiabatic and heated cases follows

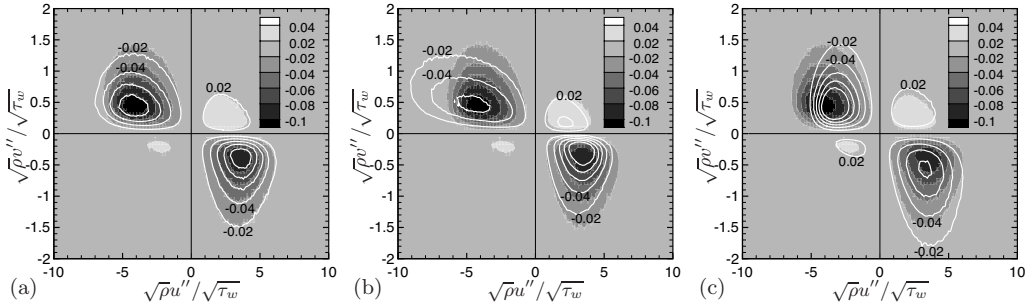

FIGURE 4. Joint probability density function at $y^\star \approx 15$ of $\sqrt{\rho}u''/\sqrt{\tau_w}$ and $\sqrt{\rho}v''/\sqrt{\tau_w}$ with contours of probability-weighted Reynolds shear stress $\rho u''v''/\tau_w P(\sqrt{\rho}u''/\sqrt{\tau_w}, \sqrt{\rho}v''/\sqrt{\tau_w})$ for cases (a) $\mathrm{CRe}_\tau^\star 2$, (b) GL and (c) LL (all lines) compared with case CP395 (filled contours).

the incompressible profile closely, the cooled case shows deviation. Using $\overline{u}^\star$ provides a universal profile for all three cases; however, a slight increase in the log-law constant is noticeable.

3.2. *Modulation in Reynolds stress generation mechanisms due to* $\mathrm{Re}_\tau^\star$ *gradients*

Besides the changes of the viscous length scale observed above, gradients of $\mathrm{Re}_\tau^\star$ also affect turbulence structure, which is related to turbulence anisotropy and Reynolds stress generation mechanisms. These changes can be seen by plotting the weighted joint probability density function (JPDF) $\left(\rho u''v'' P(\sqrt{\rho}u''/\sqrt{\tau_w}, \sqrt{\rho}v''/\sqrt{\tau_w})\right)/\tau_w$, where $P(\sqrt{\rho}u''/\sqrt{\tau_w}, \sqrt{\rho}v''/\sqrt{\tau_w})$ is the JPDF of $\sqrt{\rho}u''/\sqrt{\tau_w}$ and $\sqrt{\rho}v''/\sqrt{\tau_w}$. Figure 4 shows the contours of the weighted JPDF, where the filled contour depicts case CP395 and the contour lines correspond to cases $\mathrm{CRe}_\tau^\star 2$, GL and LL, respectively. While the case $\mathrm{CRe}_\tau^\star 2$ shows contours similar to those for case CP395, the contour lines for cases with $\mathrm{Re}_\tau^\star$ gradients show deviations. It can be seen that for case GL, the low-speed streaks strengthen and do not lift as intensely. The opposite is true for case LL. The influence of the structural changes on the mixing length in the near-wall region is too small to affect the validity of the derived velocity scaling.

3.3. *Significance of effects due to individual density and viscosity gradients*

The significance of additional mechanisms that may arise due to property fluctuations in addition to very large density or viscosity gradients is discussed next. The cases $\mathrm{CRe}_\tau^\star 1{,}2$ and 3 are ideal for investigating these additional mechanisms, because $\mathrm{Re}_\tau^\star$ is constant across the channel and equal to case CP395. We first examine the budget equations of the turbulent kinetic energy $k = \overline{\rho}\widetilde{u_i''u_i''}/2$ written as $P_k + D_k - \epsilon_k + C_k = 0$, with the production $P_k = -\overline{\rho}\widetilde{u''v''}d\tilde{u}/dy$, diffusion $D_k = d(\overline{u_i''\tau_{iy}'} - \overline{v''p'} - \overline{\rho u_i''u_i''v''})/dy$, dissipation per unit volume $\epsilon_k = -\overline{\tau_{ij}' du_i''/dx_j}$ and additional terms arising due to density fluctuations $C_k = -\overline{u_i''}d\overline{p}/dx_i + \overline{u_i''}d\overline{\tau_{iy}}/dy + \overline{p'du_i''/dx_i}$ (p is the pressure and τ_{ij} denotes the shear stress tensor). Figure 5(a) shows the dominant terms in the kinetic energy budget; namely, diffusion, dissipation and production normalized by $h/(\overline{\rho}u_\tau^{\star 3}\mathrm{Re}_\tau^\star)$ (see also Morinishi *et al.* 2004), with the semi-local friction velocity defined as $u_\tau^\star = \sqrt{\tau_w/\overline{\rho}}$. It can be seen that with increasing viscosity/density gradients ($\mathrm{CRe}_\tau^\star 1$ to $\mathrm{CRe}_\tau^\star 3$), the near-wall turbulence dissipation increases and is balanced by an increase of the diffusion. Although not shown, the contribution of the additional terms C_k remains negligible.

It is well known that density variations may result in a baroclinic torque affecting the

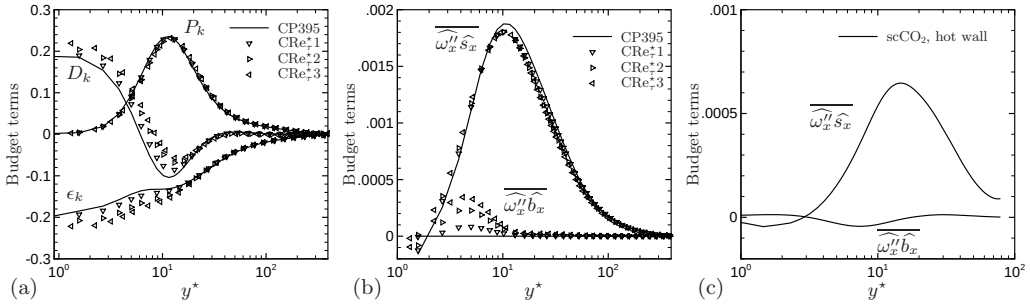

FIGURE 5. Budgets terms in (a) the turbulent kinetic energy equation for cases CP395, CRe$^\star_\tau$1, CRe$^\star_\tau$2 and CRe$^\star_\tau$3, normalized by $h/(\overline{\rho}u_\tau^{\star\,3}\mathrm{Re}^\star_\tau)$, (b) the streamwise vorticity equation for cases CP395, CRe$^\star_\tau$1, CRe$^\star_\tau$2 and CRe$^\star_\tau$3, normalized by $1/\mathrm{Re}^{\star\,3}_\tau$ and (c) the streamwise vorticity equation for scCO$_2$ cases from Peeters *et al.* (2016), normalized by $1/\mathrm{Re}^{\star\,3}_\tau$.

flow field in multiphase flows (see, for instance, Chassaing *et al.* 2002). The vorticity transport equations, using the semi-locally scaled variables, can be written as

$$\partial_{\widehat{t}}(\widehat{\rho}\widehat{\boldsymbol{\omega}}) + \widehat{\boldsymbol{\nabla}}\cdot\widehat{\rho}\widehat{\boldsymbol{u}}\widehat{\boldsymbol{\omega}} = \widehat{\rho}\widehat{\boldsymbol{\omega}}\left(\frac{\overline{\rho}}{\rho_w}\right)^{\frac{1}{2}}\cdot\widehat{\boldsymbol{\nabla}}\boldsymbol{u}^+ + \widehat{\boldsymbol{\nabla}}\times\widehat{\boldsymbol{\nabla}}\cdot\left\{\frac{2\widehat{\mu}}{\mathrm{Re}^\star_\tau}\left(\frac{\overline{\rho}}{\rho_w}\right)^{\frac{1}{2}}\boldsymbol{S}^+\right\} - \widehat{\rho}\widehat{\boldsymbol{\omega}}\left(\frac{\overline{\rho}}{\rho_w}\right)^{\frac{1}{2}}\widehat{\boldsymbol{\nabla}}\cdot\boldsymbol{u}^+ + \frac{1}{\rho}\widehat{\boldsymbol{\nabla}}\rho\times\widehat{\boldsymbol{\phi}}, \tag{3.5}$$

where the hat denotes semi-locally scaled variables, with $\widehat{\rho}=\rho/\overline{\rho}$, $\widehat{\mu}=\mu/\overline{\mu}$, $\widehat{\boldsymbol{u}}=\boldsymbol{u}/u^\star_\tau$, $\widehat{\boldsymbol{\omega}}=\boldsymbol{\omega}h/u^\star_\tau$, $\widehat{\boldsymbol{\nabla}}=h\boldsymbol{\nabla}$, $\widehat{\boldsymbol{\phi}}\equiv\widehat{\boldsymbol{\nabla}}\widehat{p}-\widehat{\boldsymbol{\nabla}}\cdot(2\widehat{\mu}/\mathrm{Re}^\star_\tau\,(\overline{\rho}/\rho_w)^{\frac{1}{2}}\,\boldsymbol{S}^+)$, $\widehat{p}=p/(\overline{\rho}u^{\star\,2}_\tau)$ and $\boldsymbol{S}^+=(\widehat{\boldsymbol{\nabla}}\boldsymbol{u}^+)+(\widehat{\boldsymbol{\nabla}}\boldsymbol{u}^+)^{\mathrm{T}}-\frac{1}{3}(\widehat{\boldsymbol{\nabla}}\cdot\boldsymbol{u}^+)\boldsymbol{I}$ is the strain rate tensor. The physical significance of the terms on the right-hand side can be seen as the production of vorticity due to stretching and tilting, diffusion of vorticity, production or destruction of vorticity due to thermal expansion, and production or destruction due to density gradients. We will refer to $\rho^{-1}\widehat{\boldsymbol{\nabla}}\rho\times\widehat{\boldsymbol{\phi}}$ as the baroclinic source term $\widehat{\boldsymbol{b}}$. The last two terms on the right-hand side are zero in a constant-density flow, since they only appear because of density variations. This is also the reason why these two terms cannot be incorporated in the semi-local scaling framework. This also suggests that very large (instantaneous) density gradients may lead to situations in which the semi-local scaling would no longer be valid. To investigate the baroclinic effect, we calculated the budgets of the streamwise vorticity. These budgets are obtained by decomposing all variables of the streamwise component of Eq. (3.5) in a Favre-averaged part $\widetilde{(...)}$ and a fluctuating part $(...)''$, then multiplying the result by the fluctuating part of the streamwise vorticity $\widehat{\omega''_x}$ and subsequently averaging with respect to time $\overline{(...)}$. These budgets can be used to compare the magnitude of baroclinicity $\overline{\widehat{\omega''_x}\widehat{b_x}}$ with the magnitude of the stretching and tilting term $\overline{\widehat{\rho}\widehat{\omega''_x}\widehat{\boldsymbol{\omega}}\,(\overline{\rho}/\rho_w)^{\frac{1}{2}}\cdot\widehat{\boldsymbol{\nabla}}u^+}$, which we shall denote $\overline{\widehat{\omega''_x}\widehat{s_x}}$. Figure 5(b) shows both $\overline{\widehat{\omega''_x}\widehat{b_x}}$ and $\overline{\widehat{\omega''_x}\widehat{s_x}}$ normalized by $1/\mathrm{Re}^{\star\,3}_\tau$ for the cases CRe$^\star_\tau$1,2 and 3 compared with case CP395. It is clear from Figure 5(b) that the stretching/tilting term scales well using the semi-local scaling, while the baroclinicity increases with increasing property gradients. The effect of baroclinicity is confined mostly to the near-wall region ($y^\star<10$). Furthermore, its magnitude is small compared to that of the stretching/tilting term. Figure 5(c) shows similar results for the forced convection scCO$_2$ case. Note that the sign of the baroclinic effect in the scCO$_2$ case is opposite to

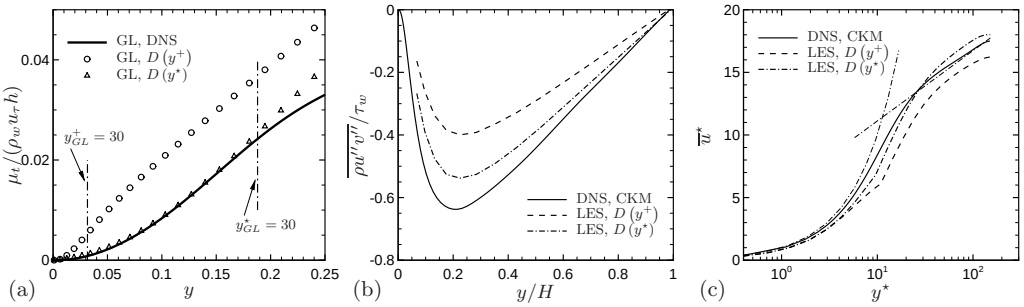

FIGURE 6. (a) Eddy viscosity μ_t for the cases GL compared to mixing length models that use either y^+ or $y^\star$ as the normalized wall distance in the ad hoc damping function D, (b) turbulent shear stress $\overline{\rho u'' v''}$ and (c) semi-locally transformed mean velocity $u^\star$ from LES with either $D\left(y^+\right)$ or $D\left(y^\star\right)$ compared to DNS of Coleman *et al.* (1995) abbreviated as CKM.

that of the $\mathrm{CRe}^\star_\tau$ cases, because the flow in the $\mathrm{scCO_2}$ case is heated, whereas the flow in the $\mathrm{CRe}^\star_\tau$ cases is cooled.

3.4. *Wall-modeled LES of a* $\mathrm{M} = 3$ *turbulent channel flow*

Based on the scaling law for velocity and the scaling of the turbulent statistics discussed above, it is now possible to revisit turbulence models that are commonly used in wall-modeled LES and RANS. Arguably, the simplest turbulence model that can be considered is the eddy viscosity model based on Prandtl's mixing length hypothesis. Such an eddy viscosity model can be written as

$$\mu_t = \kappa y \rho u^\star_\tau D^2, \tag{3.6}$$

with D an ad hoc van Driest damping function for the near-wall region, given by

$$D\left(y^+\right) = 1 - \exp\left(-y^+/A^+\right). \tag{3.7}$$

The model parameters are $\kappa = 0.41$ and $A^+ = 17$. Using $u^\star_\tau$ in Eq. (3.6) accounts for changes in the velocity scales due to mean density gradients. However, using y^+ implicitly assumes that the viscous length scales are not affected by property gradients and are thus the same for a constant-property flow. Simply replacing y^+ with $y^\star$ in Eq. (3.7) corrects for changes in viscous length scales in variable-property flows due to gradients in $\mathrm{Re}^\star_\tau$. This is highlighted in Figure 6(a), where the eddy viscosity $\mu_t = -\overline{\rho u'' v''}/(d\bar{u}/dy)$ obtained from DNS for the case GL is compared with Eq. (3.6) using either y^+ or $y^\star$ as the argument in the damping function. It can be clearly seen that the model with $D(y^\star)$ closely follows the DNS. Although not shown, similar improvements are obtained for the case LL. The figure also indicates the wall-normal locations where y^+ and $y^\star$ equals 30 to highlight again the significant changes of viscous scales for case GL. The effectiveness of the semi-local scaling to accommodate changes in viscous length scales was also evident for the Kolmogorov and mixing length profiles in Figure 2(b,c). Bocquet *et al.* (2012) suggested a similar modification of the wall distance scaling in the van Driest damping function in order to accommodate compressibility effects in supersonic channel flows.

To test the suggested modification of the damping function, we performed a wall-modeled LES of a $\mathrm{M} = 3$ compressible channel flow with cold isothermal walls as documented in Coleman *et al.* (1995). The LES code INCA (Hickel *et al.* 2014) was used and an equilibrium wall model, which makes use of the eddy viscosity model as given in Eq. (3.6), was implemented during the summer program. For the sake of complete-

ness we briefly outline the implementation hereafter. The equilibrium boundary layer equations for momentum ($\partial_y\left(\mu+\mu_t\right)\partial_y\widetilde{u}=0$) and total energy ($\partial_y\widetilde{u}\left(\mu+\mu_t\right)\partial_y\widetilde{u}+\partial_y\left(\mu/\mathrm{Pr}+\mu_t/\mathrm{Pr}_t\right)c_p\partial_y\widetilde{T}=0$) are solved using a Newton-type iteration procedure. A second-order finite-difference scheme, with analytic transformations to incorporate mesh stretching, is used to discretize the spatial derivatives. $\widetilde{u}$ and $\widetilde{T}$ are the filtered streamwise velocity and temperature, while $\mathrm{Pr}=0.7$ and $\mathrm{Pr}_t=0.9$ are the molecular and turbulent Prandtl numbers, respectively. The coupling between LES and the equilibrium wall model follows a standard procedure, whereby the numerical solution of the equilibrium boundary layer equations provides the wall boundary conditions for the LES (in the form of viscous and thermal fluxes); and the LES provides the boundary conditions for velocity and enthalpy at a location of $y^\star\approx 30$ for the numerical integration of the boundary layer equations. Note the choice of $y^\star$, instead of y^+, to define the coupling point between LES and boundary layer equations. Twelve mesh points are used for the integration of the boundary layer equations and the LES uses 24 control volumes in the wall-normal direction and a mesh resolution of Δx^+ and Δz^+ of 120 and 83 at the wall, respectively.

4. Conclusions

The LES results for the turbulent shear stress $\overline{\rho u''v''}$ and the transformed velocity $\bar{u}^\star$ are compared to the DNS of Coleman *et al.* (1995) in Figure 6(b,c). It can be clearly seen that the simple correction for the damping function in Eq. (3.7), where we replaced y^+ with $y^\star$, significantly improves the results for the turbulent shear stress. Accordingly, the velocity profiles are also close to those of the DNS. However, cases with higher Reynolds numbers will be tested in the future to thoroughly assess the validity of suggested modifications. We investigated wall-bounded turbulent flows with strong variations in density and viscosity to verify if the semi-local Reynolds number can be used as a universal parameter to characterize turbulent statistics and to collapse mean velocity profiles. The cases analyzed are volumetrically heated channel flows with isothermal walls, heated and cooled annular flows with carbon dioxide at supercritical pressure, and heated and cooled supersonic boundary layer flows. We showed that velocity profiles for these cases can be collapsed if the mean velocity is transformed as a function of the semi-local Reynolds number. Also, the turbulence statistics in the budget equations of the turbulence kinetic energy and streamwise vorticity equation are governed by $\mathrm{Re}_\tau^\star$. However, for strong density gradients, baroclinicity is increasing in magnitude, which cannot be incorporated in the semi-local scaling framework. Large gradients of viscosity (and density) also cause turbulence dissipation to deviate slightly from the constant-property case, even if scaled by semi-local scales. These observations enabled us to revisit and correct a simple eddy viscosity model (based on the mixing length hypothesis) to account for strong thermophysical property gradients. Simply replacing the normalized wall distance y^+ (based on wall units) with the semi-local wall distance $y^\star$ significantly improves the results obtained by a wall-modeled LES of a turbulent channel flow at $\mathrm{M}=3$ with isothermal walls. The knowledge obtained in this work can further be utilized to correct and properly account for property gradients in more complex turbulence models used in LES and RANS.

REFERENCES

Bocquet, S., Sagaut, P. & Jouhaud, J. 2012 A compressible wall model for large-

eddy simulation with application to prediction of aerothermal quantities. *Phys. Fluids.* **24** (6), 065103.

Chassaing, P., Antonia, R., Anselmet, F., Joly, L. & Sarkar, S. 2002 *Variable density fluid turbulence*. Kluwer.

Coleman, G. N., Kim, J. & Moser, R. D. 1995 A numerical study of turbulent supersonic isothermal-wall channel flow. *J. Fluid Mech.* **305**, 159–183.

Duan, L., Beekman, I. & Martin, M. P. 2010 Direct numerical simulation of hypersonic turbulent boundary layers. Part 2. Effect of wall temperature. *J. Fluid Mech.* **655**, 419–445.

Foysi, H., Sarkar, S. & Friedrich, R. 2004 Compressibility effects and turbulence scalings in supersonic channel flow. *J. Fluid Mech.* **509**, 207–216.

Hickel, S., Egerer, C. P. & Larsson, J. 2014 Subgrid-scale modeling for implicit large-eddy simulation of compressible flows and shock-turbulence interaction. *Phys. Fluids.* **26** (10), 106101.

Huang, P. G., Coleman, G. N. & Bradshaw, P. 1995 Compressible turbulent channel flows: DNS results and modelling. *J. Fluid Mech.* **305**, 185–218.

Lee, J., Yoon Jung, S., Jin Sung, H. & Zaki, T. A. 2013 Effect of wall heating on turbulent boundary layers with temperature-dependent viscosity. *J. Fluid Mech.* **726**, 196–225.

Modesti, D. & Pirozzoli, S. 2016 Reynolds and Mach number effects in compressible turbulent channel flow. *Int. J. Heat Fluid Fl.* **59**, 33–49.

Morinishi, Y., Tamano, S. & Nakabayashi, K. 2004 Direct numerical simulation of compressible turbulent channel flow between adiabatic and isothermal walls. *J. Fluid Mech.* **502**, 273–308.

Morkovin, M. V. 1962 Effects of compressibility on turbulent flows. *In Mecanique de la Turbulence, ed. A. Favre*, 367–380.

Najm, H. N., Wyckoff, P. S. & Knio, O. M. 1998 A semi-implicit numerical scheme for reacting flow: I. Stiff chemistry. *J. Comp. Phys.* **143** (2), 381–402.

Nemati, H., Patel, A., Boersma, B. J. & Pecnik, R. 2016 The effect of thermal boundary conditions on forced convection heat transfer to fluids at supercritical pressure. *J. Fluid Mech.* **800**, 531–556.

Patel, A., Boersma, B. J. & Pecnik, R. 2016 The influence of near-wall density and viscosity gradients on turbulence in channel flows. *J. Fluid Mech.* **809**, 793–820.

Patel, A., Peeters, J. W. R., Boersma, B. J. & Pecnik, R. 2015 Semi-local scaling and turbulence modulation in variable property turbulent channel flows. *Phys. Fluids.* **27**, 095101.

Peeters, J. W. R., Pecnik, R., Rohde, M., van der Hagen, T. H. J. J. & Boersma, B. J. 2016 Turbulence attenuation in simultaneously heated and cooled annular flows at supercritical pressure. *J. Fluid Mech.* **799**, 505–540.

Shadloo, M., Hadjadj, A. & Hussain, F. 2015 Statistical behavior of supersonic turbulent boundary layers with heat transfer at $M_\infty = 2$. *Int. J. Heat Fluid Fl.* **53**, 113–134.

Smits, A. J. & Dussauge, J.-P. 2006 *Turbulent shear layers in supersonic flow*. Springer Science & Business Media.

Trettel, A. & Larsson, J. 2016 Mean velocity scaling for compressible wall turbulence with heat transfer. *Phys. Fluids.* **28**, 026102.